Supplementary Information

Highly Stable Color-Tunable Organic Long-Persistent Luminescence from a Single-component Copolymer for Vitro Antibacterial

Hui Li,[*a] Xiaoye Li,[b] Haoran Su,[a] Shuman Zhang,[a] Cheng Tan,[a] Cheng Chen,[a] Xin Zhang,[a] Jiani Huang,[a] Jie Gu,[a] Huanhuan Li,[a] Gaozhan Xie,[a] Heng Dong,[*b] Runfeng Chen[a] and Ye Tao[*ac]

Dr. H. Li, Mr. H. R. Su, Ms. S. M. Zhang, Mr. C. Tan, Mr. C. Chen, Ms. X. Zhang, Ms. J. N. Huang, Ms. J. Gu, Dr. H. H. Li, Dr. G. Z. Xie, Prof. R. F. Chen, and Prof. Y. Tao

[a]State Key Laboratory of Organic Electronics and Information Displays & Institute of Advanced Materials (IAM), Nanjing University of Posts & Telecommunications, 9 Wenyuan Road, Nanjing 210023, China.

E-mail: iamhli@njupt.edu.cn; iamytao@njupt.edu.cn.

Mr. X. Y. Li, Dr. H. Dong

[b]Nanjing Stomatological Hospital, Affiliated Hospital of Medical School, Research Institute of Stomatology, Nanjing University, 30 Zhongyang Road, Nanjing, Jiangsu 210008, China.

E-mail: dongheng90@smail.nju.edu.cn.

Prof. Y. Tao

[c]Songshan Lake Materials Laboratory, Dongguan, Guangdong 523808, China.

Content

1. Synthesis and characterization

Materials: All reagents, unless otherwise specified, were purchased from Aldrich, Acros or Alfa Aesar, and used without further purification. Manipulations involving air-sensitive reagents were performed in an atmosphere of dry argon (Ar).

Instruments: ^{1}H and ^{13}C-nuclear magnetic resonance (NMR) spectra were recorded on Bruker Ultra Shield Plus 400 MHz instruments with DMSO-d_6 and $CDCl_3$ as the solvents and tetramethylsilane (TMS) as the internal standard. Molecular weights of the polymers were measured by gel permeation chromatography (GPC) on Waters 410 with polystyrene as the standard and THF as the eluent. Fourier transform infrared spectroscopy (FTIR) spectra were obtained by using Perkin Elmer Spectrum Two IR instrument with potassium bromide pellet.

Synthesis of N,N-dimethyl-4'-vinyl-[1,1'-biphenyl]-4-amine (DMB)

4-Vinylphenylboronic acid (1.48 g, 10 mmol), 4-bromo-N,N-dimethylaniline (2.00 g, 10 mmol), tetrakis(triphenylphosphine) palladium (0.35 g, 0.3 mmol) and toluene (20 mL) were mixed and stirred under Ar atmosphere. Subsequently, K_2CO_3 aqueous solution (3 mL, 2 mol/L) in which oxygen has been removed with Ar was rapidly added to the reaction mixture. After stirring at 90°C for 48 h, the mixture was quenched by 10 mL water, and extracted with dichloromethane (3×30 mL). The organic layers were collected and dried with anhydrous sodium sulfate (Na_2SO_4) and purified by column chromatography to give **DMB**. Yield: 1.81 g of yellow-green powder (81%).^{1}H NMR (400 MHz, DMSO-d_6, ppm): δ 7.60-7.47 (m, 6H), 6.82-6.78 (m, 2H), 6.78-6.70 (m, 1H), 5.86-5.79 (m, 1H), 5.24 (d, J=11.8 Hz, 1H), 2.95 (s, 6H). ^{13}C NMR (100 MHz, $CDCl_3$): δ 136.56, 127.51, 126.55, 126.22, 113.04, 112.73, 53.42, 40.56.

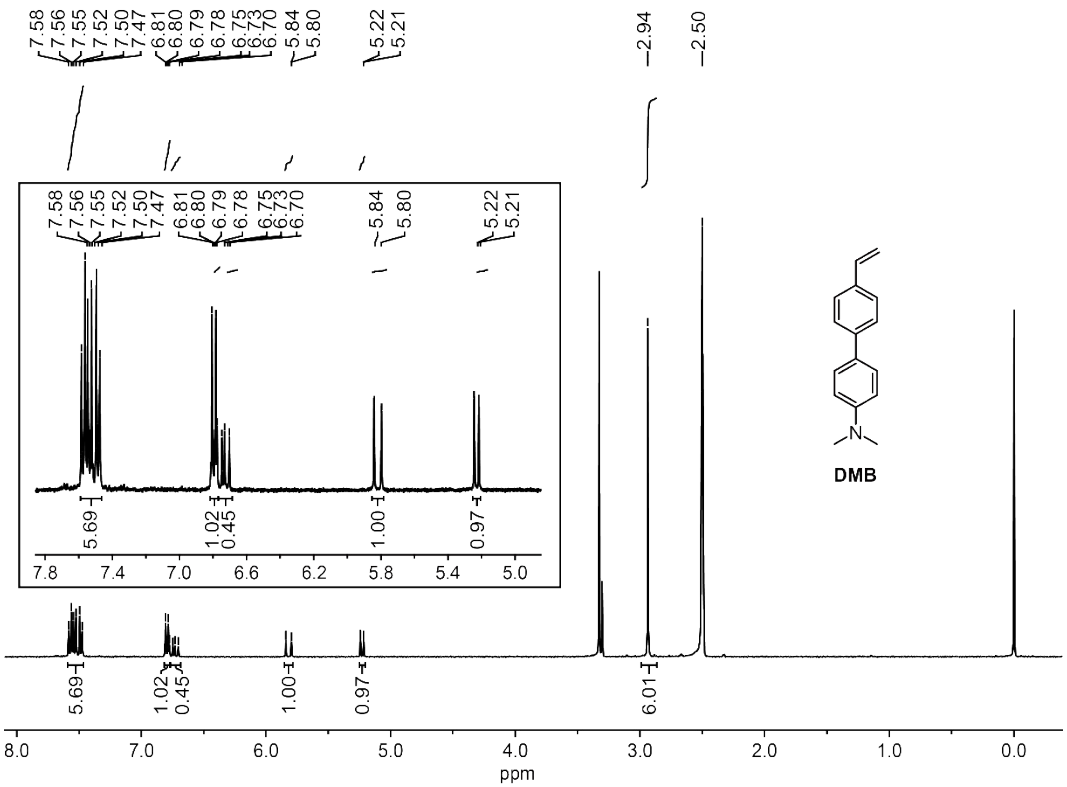

Figure S1. ^{1}H NMR spectrum of **DMB** in DMSO-d_6.

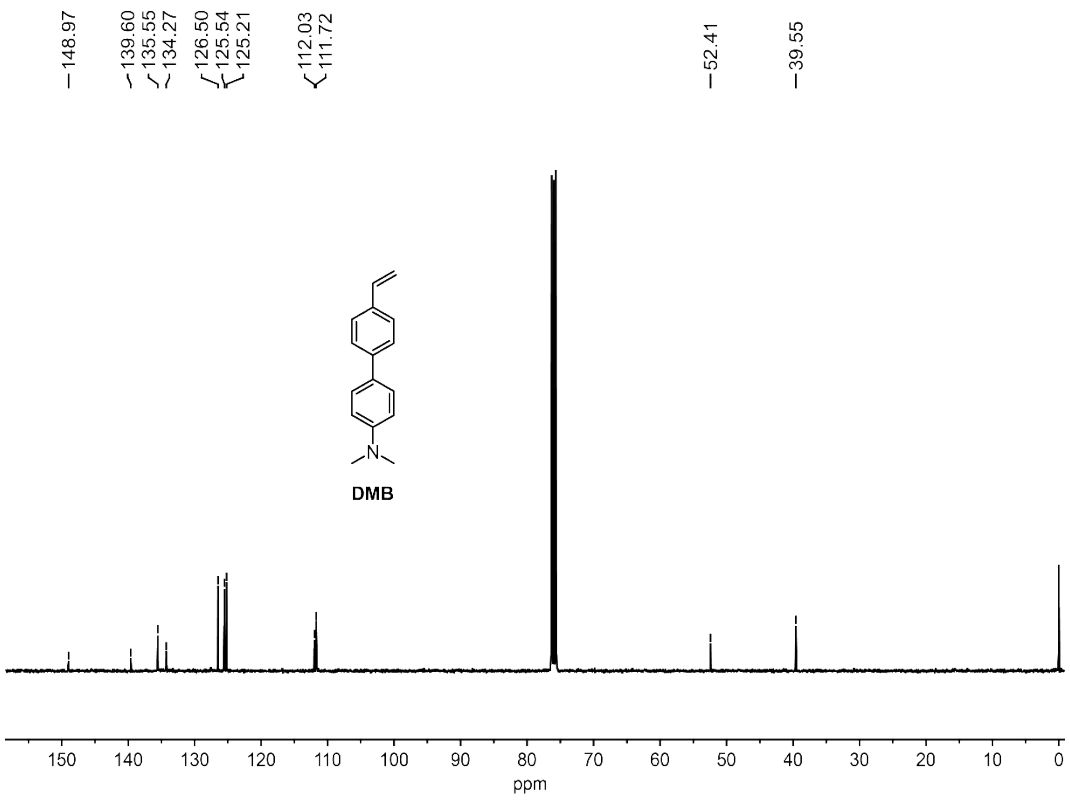

Figure S2. ^{13}C NMR spectrum of **DMB** in $CDCl_3$.

Synthesis of diphenyl(4-vinylphenyl) phosphane (DPPO)

1-Bromo-4-vinylbenzene (0.92 g, 5 mmol) was dissolved in 40 mL dry THF using a syringe under an Ar atmosphere. The solution was cooled to -78ºC in a dry ice/acetone bath and stirred for 10 min, and then a 10 M hexane solution of *n*-butyllithium (0.8 mL, 5.5 mmol) was added into slowly. After stirring at -78ºC for 1 h, chlorodiphenylphosphine (1.48 mL, 8.06 mmol) was added to give a clear yellow solution, and the reaction mixture was stirred for 1 h at -78°C then the dry ice/acetone bath was removed and reacted overnight. And 5 mL of 30% hydrogen peroxide (H_2O_2) was added into the mixture slowly and reacted overnight. Then the solvent was removed under reduced pressure to give the off-white solid. It was digested in methanol, filtered, digested in water, and filtered. The crude material was purified by column chromatography to give **DPPO**. Yield: 0.78 g of white powder (51%). ^{1}H NMR (400 MHz, DMSO-d_6): δ 7.56-7.16 (m, 14H), 6.74 (dd, J=17.7, 11.0 Hz, 1H), 5.88 (dd, J=17.7, 0.8 Hz, 1H), 5.32 (dd, J=10.9, 0.7 Hz, 1H). ^{13}C NMR (100 MHz, $CDCl_3$): δ 141.14, 135.91, 132.84, 132.47, 132.13, 132.03, 130.78, 128.62, 126.20, 116.65.

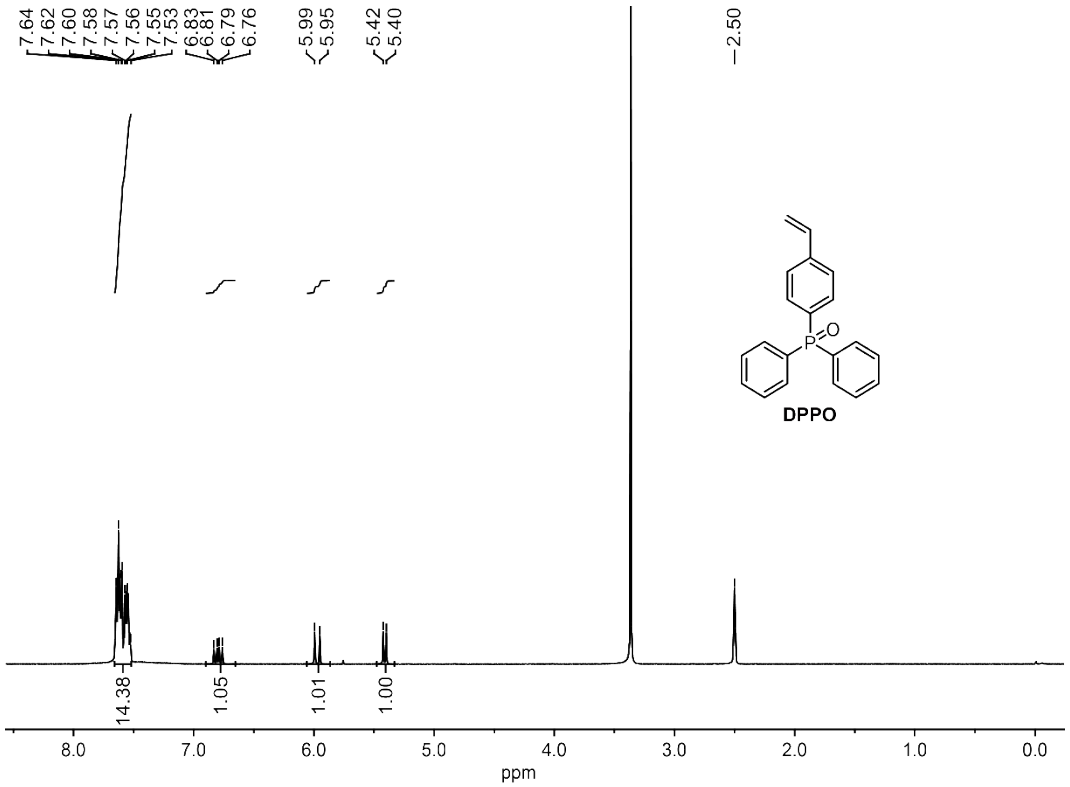

Figure S3. ^{1}H NMR spectrum of **DPPO** in DMSO-d_6.

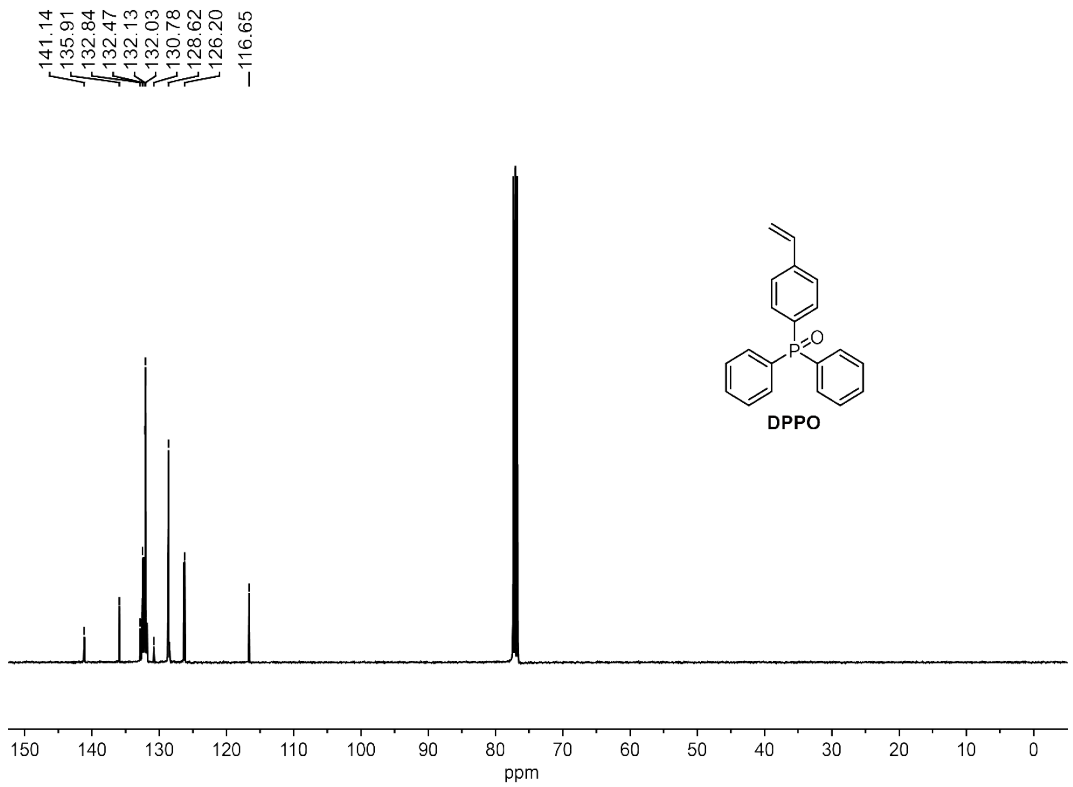

Figure S4. ^{13}C NMR spectrum of **DPPO** in $CDCl_3$.

Synthesis of PDDs

Radical copolymerization of N,N-dimethyl-4'-vinyl-[1,1'-biphenyl]-4-amine (**DMB**) and diphenyl(4-vinylphenyl)phosphane (**DPPO**) was employed by introducing azodiisobutyronitrile (AIBN) as the radical initiator under nitrogen atmosphere in N,N-dimethylformamide. Wrap the whole process in tin foil and keep it away from light. The mixture was heated to 40℃, then increase the temperature by 10℃ every 10 min. When the temperature is stable at 70℃, continue stirring for 20 h. The product was dialyzed in deionized water through a dialysis bag, and then dried in a vacuum oven. The faint yellow powder was got after removing small molecular by extracting with petroleum ether.

PDD-99: **DMB** (2 mg, 0.0089 mmol), **DPPO** (269 mg, 0.887 mmol) and AIBN (14.596 mg, 0.089 mmol) were used in the polymerization.

PDD-199: **DMB** (2 mg, 0.0089 mmol), **DPPO** (538 mg, 1.771 mmol) and AIBN (29.192 mg, 0.178 mmol) were used in the polymerization.

PDD-299: **DMB** (2 mg, 0.0089 mmol), **DPPO** (808 mg, 2.661 mmol) and AIBN (43.788 mg,

0.267 mmol) were used in the polymerization.

Synthesis of P-DPPO

P-DPPO was prepared under the identical synthetic conditions described in the preparation of **PDD**s using **DPPO** (5.0 g, 30 mmol), AIBN (1.4 g, 36 mmol), DMF (50 mL) for white powder.

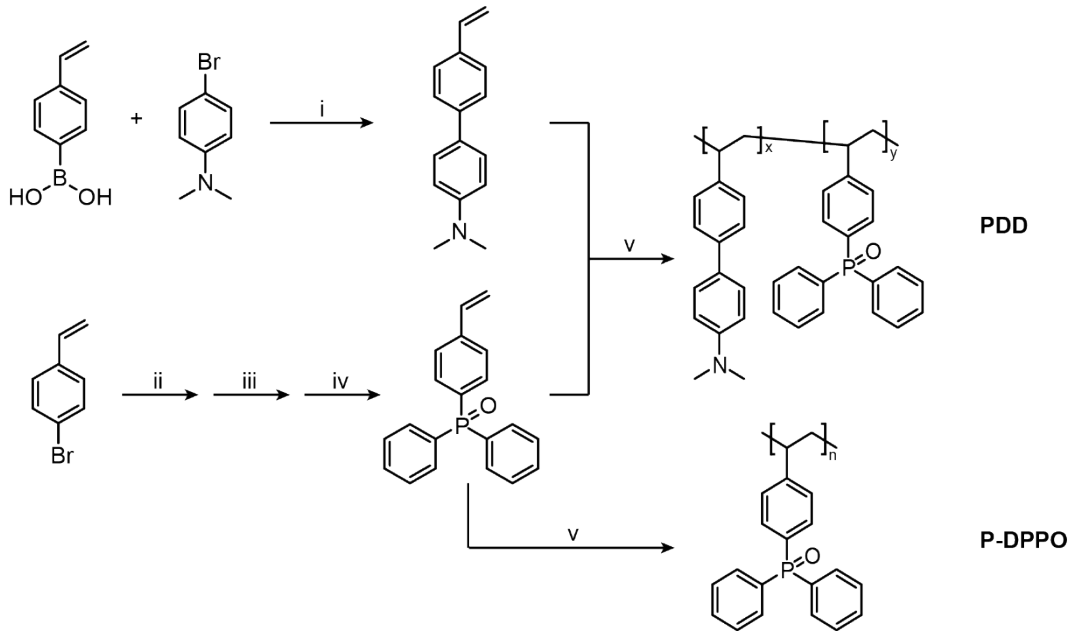

Scheme S1. Synthetic routes of **DMB**, **DPPO**, **PDD**s and **P-DPPO**. (i) tetrakis(triphenylphosphine) palladium, K_2CO_3, toluene, 90℃, 48 h; (ii) *n*-BuLi, THF, -78℃, 1 h; (iii) chlorodiphenylphosphine, -78℃, 1 h; (iv) 30% H_2O_2, room temperature, overnight. (v) AIBN, DMF, 70°C, 20 h.

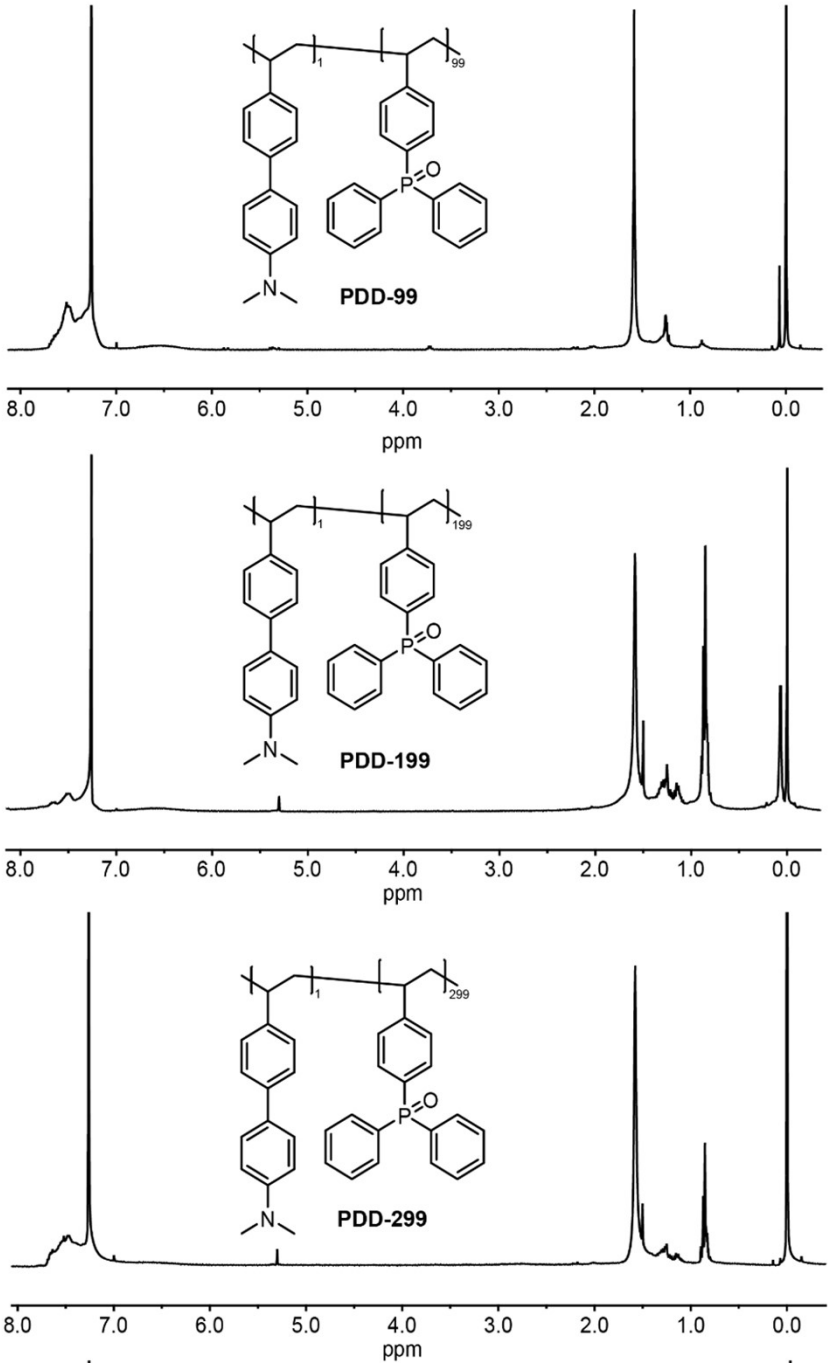

Figure S5. ^{1}H NMR spectra of **PDD-99/199/299** in $CDCl_3$.

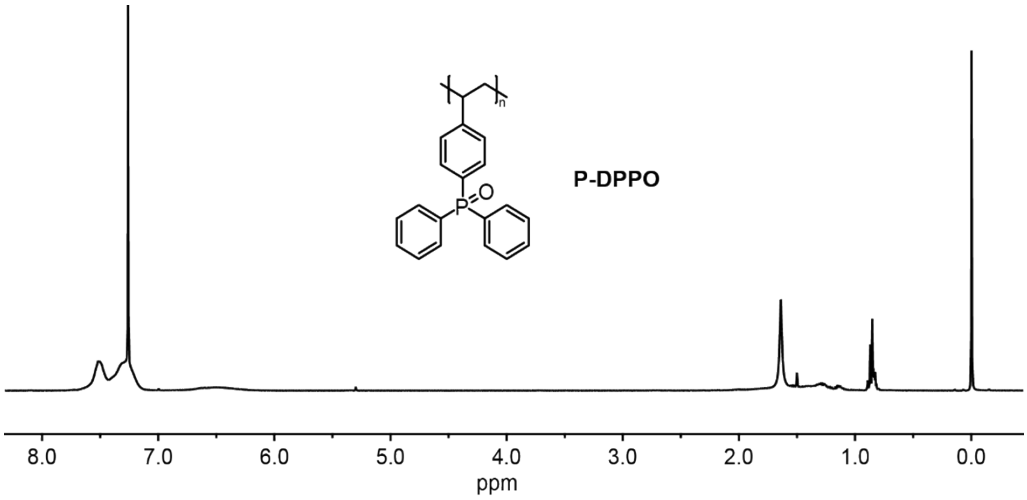

Figure S6. ^{1}H NMR spectrum of **P-DPPO** in $CDCl_3$.

Table S1. Characterizations of polymers.

Sample	**PDD-99**	**PDD-199**	**PDD-299**	**P-DPPO**
M_w (Da)	9217	16390	15480	8658
M_n (Da)	6894	15342	13921	6250
PDI	1.34	1.07	1.11	1.39

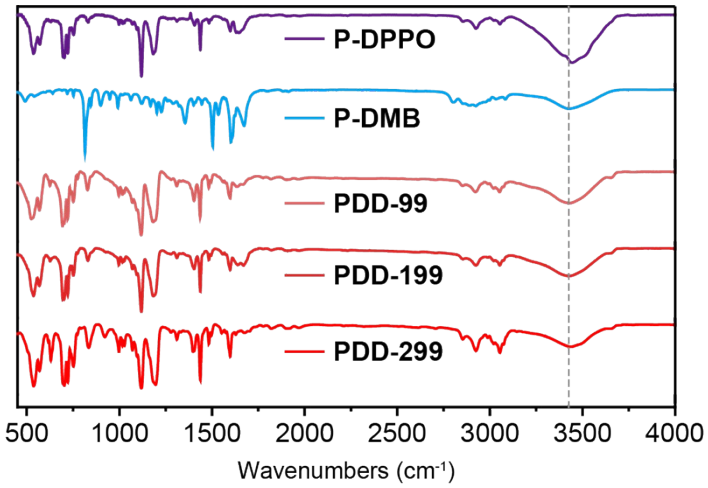

Figure S7. FTIR spectra of **P-DPPO**, **P-DMB** and **PDD**s. The presence of a signal intensity similar to that of **P-DMB** at 3428 cm^{-1} indicates the successful incorporation of the donor unit **DMB** into the copolymer system.

2. Powder XRD analysis

Powder X-ray diffraction (XRD) patterns were recorded on a Rigaku D/max 2250VB/PC diffraction with Cu-Kα radiation (λ=1.5406 Å).

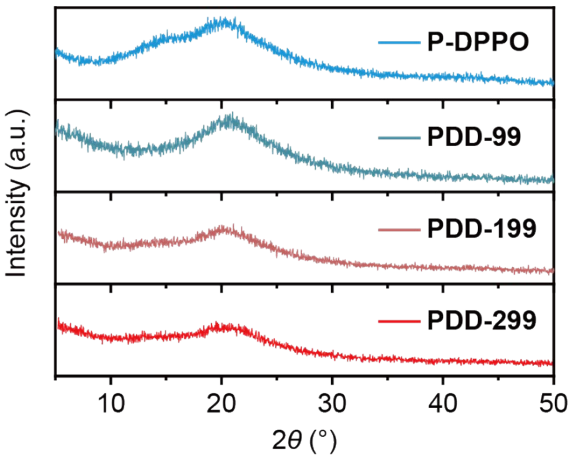

Figure S8. Powder XRD patterns of **P-DPPO** and **PDD**s powders.

3. Thermal properties

Thermogravimetric analyses (TGA) were conducted on a DTG-60 Shimadzu thermal analyst system under a heating rate of 10ºC/min and a nitrogen flow rate of 50 cm^3/min. The differential scanning calorimetry (DSC) analyses were performed on a Shimadzu DSC-60A instrument under a heating rate of 10ºC/min and a nitrogen flow rate of 20 cm^3/min.

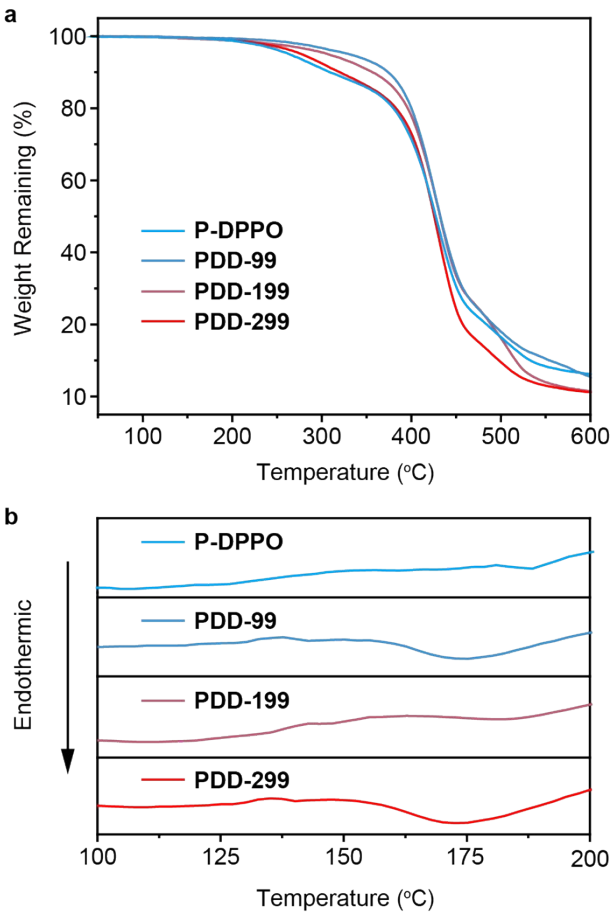

Figure S9. TGA (a) and DSC (b) curves of **P-DPPO** and **PDD-99/199/299**.

4. Electrochemical properties

To investigate the electrochemical properties of the compounds, cyclic voltammogram (CV) measurements were performed at room temperature on a CHI660E system in a typical three-electrode cell with a working electrode (glass carbon), a reference electrode (Ag/Ag^+, referenced against ferrocene/ferrocenium (FOC)), and a counter electrode (Pt wire) in an acetonitrile solution of tetrabutylammonium hexafluorophosphate (Bu_4NPF_6) (0.1 M) at a sweeping rate of 100 mV s^{-1}. The highest occupied molecular orbital (HOMO) energy levels (E_{HOMO}) of the materials are estimated based on the reference energy level of ferrocene (4.8 eV below the vacuum) according to the Equations S1:

$$E_{\mathrm{HOMO}} = -\left[E_{onset}^{Ox} - (0.04)\right] - 4.8eV \quad \text{(S1)}$$

Where 0.04 V is the onset oxidative voltage of FOC vs Ag/Ag^+ and E_{onset}^{Ox} is the onset potentials of the oxidation wave of the materials deposited as thin films on the surface of the working electrode. The lowest unoccupied molecular orbital (LUMO) energy levels (E_{LUMO}) were estimated by adding the optical bandgap (E_g) to the corresponding HOMO energy level as in Equation S2:

$$E_{\mathrm{LUMO}} = E_{\mathrm{HOMO}} + E_{\mathrm{g}} \quad \text{(S2)}$$

E_g was calculated from the onset thresholds of the absorption spectra.

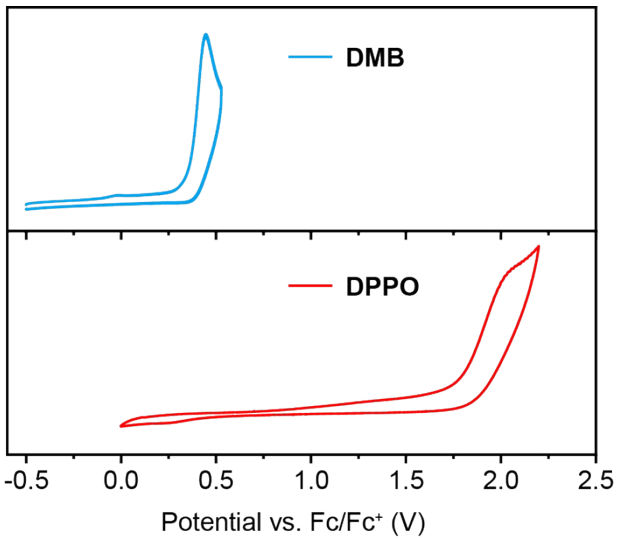

Figure S10. Cyclic voltammograms of **DMB** and **DPPO**.

Table S2. The electrochemical properties of **DMB**, **DPPO**.

Parameters	CV (eV)		
	HOMO	LUMO	E_g
DMB	-5.08	-1.52	3.56
DPPO	-6.54	-2.91	3.63

5. Theoretical calculations

Density functional theory (DFT) and time-dependent DFT (TD-DFT) simulations were performed on the Gaussian 09 package. The ground state geometries were optimized by DFT method of Becke's three-parameter exchange functional along with the Lee Yang Parr's correlation functional (B3LYP)/6-31G(d). The optimized static point was further carried out by harmonic vibration frequency analysis to guarantee that the real local minimum was achieved. The frontier molecular orbital distributions and the HOMO and LUMO energy levels were predicted and calculated by B3LYP/6-31G(d) based on the optimized ground state (S_0) geometries, respectively. The excitation energy of the lowest singlet state (S_1) and the *n*-th triplet state (T_n) states were calculated by TD-DFT method of B3LYP/6-31G(d) based on the monomer and selected dimer from the reported single crystal of triphenylphosphine oxide. Dalton program with quadratic response function method was used to predict spin-orbit coupling (SOC) matrix elements between S_1 and T_n. The single molecular and dimer SOC values of triphenylphosphine oxide were carried out using B3LYP functional and cc-pVDZ basis set on the basis of the optimized geometry of the T_1 and the ground states of the dimer in the single-crystal structures, respectively.

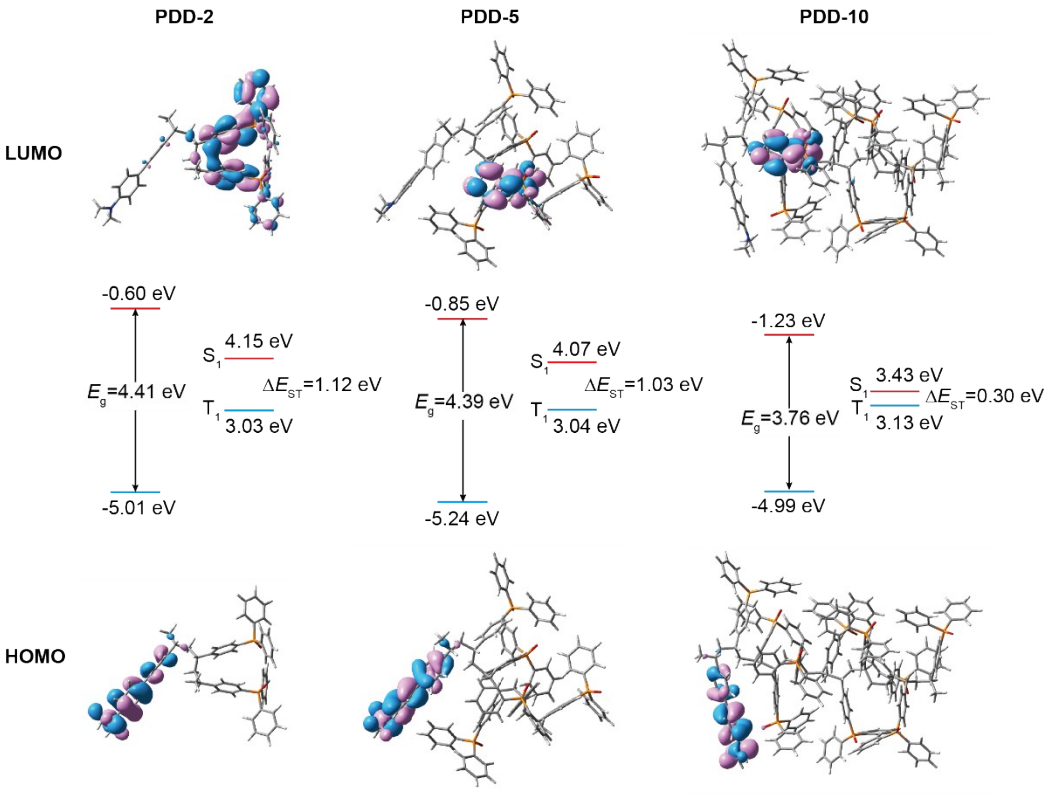

Figure S11. Frontier molecular orbital distributions, energy levels, E_g and theoretical excited state energies, ΔE_{ST} of **PDD-2**, **PDD-5** and **PDD-10**.

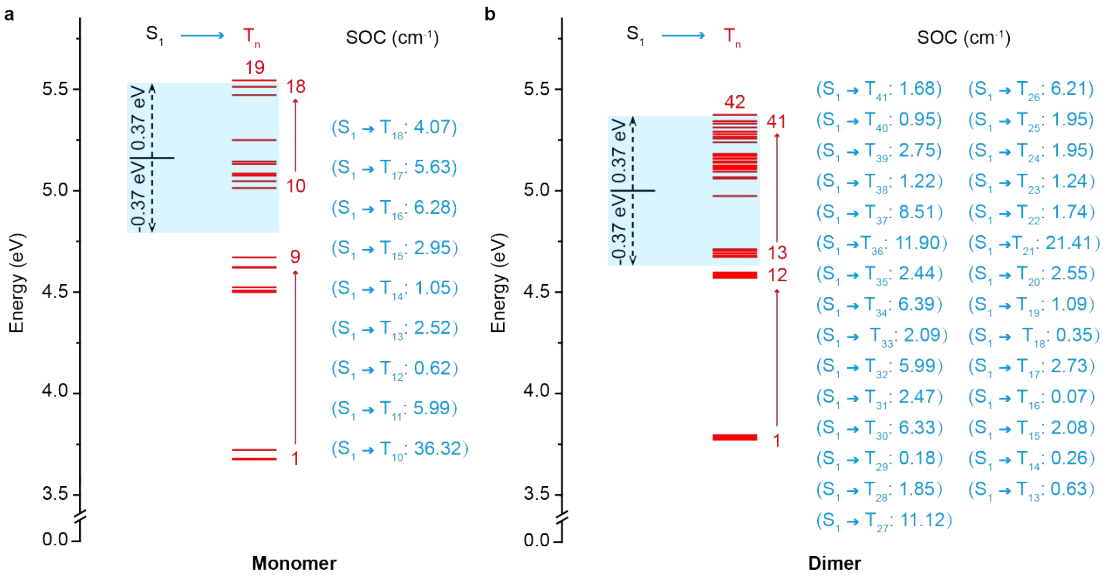

Figure S12. TD-DFT calculated energy level diagram and the corresponding SOC constants based on the molecular structures of monomer and selected dimer from triphenylphosphine oxide single crystal.

6. Photophysical investigations

Ultraviolet/visible (UV/Vis) and steady-state photoluminescence (SSPL) spectra were recorded on a Jasco V-750 spectrophotometer and Edinburgh FLS980, respectively. Phosphorescence spectra were obtained using an Edinburgh FLS980 fluorescence spectrophotometer with a 10 ms delay time after excitation using a microsecond flash lamp. The excitation spectra, OLPL (organic long-persistent luminescence) spectra and decay profiles were also measured using an Edinburgh FLS980 fluorescence spectrophotometer. Electron paramagnetic resonance (EPR) spectra was measured by BRUKER EPR instruments.

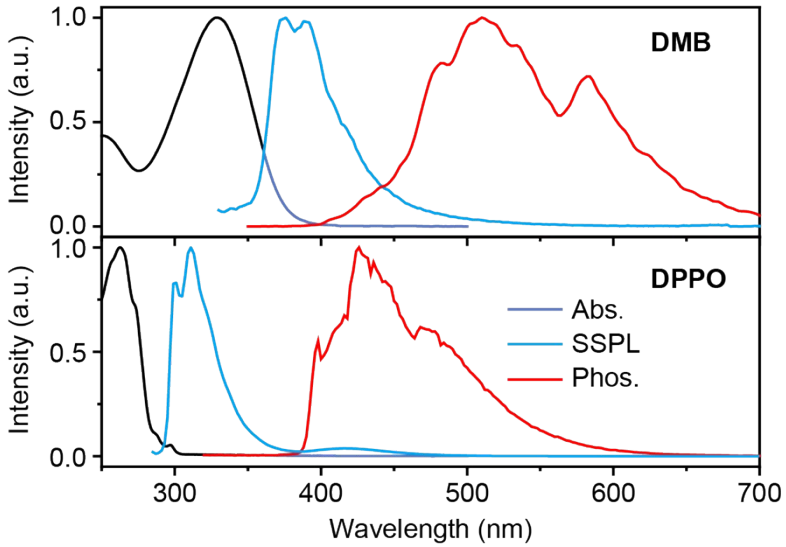

Figure S13. Absorption, SSPL and phosphorescence spectra of **DMB** and **DPPO** in dichloromethane solution (~10^{-5} mol L^{-1}).

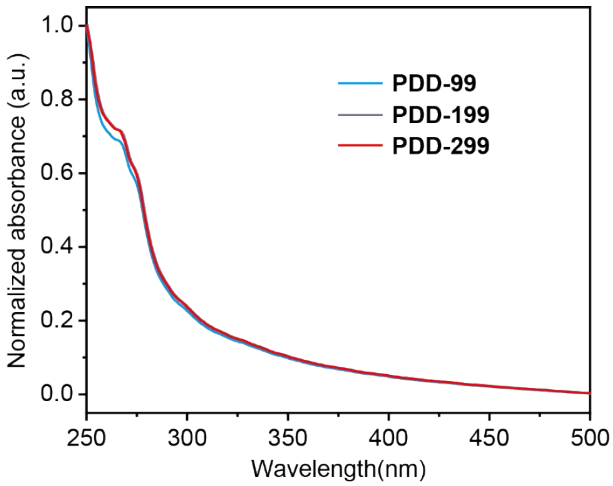

Figure S14. Absorption spectra of **PDD-99**, **PDD-199** and **PDD-299** in toluene solution (~0.5 mg/mL).

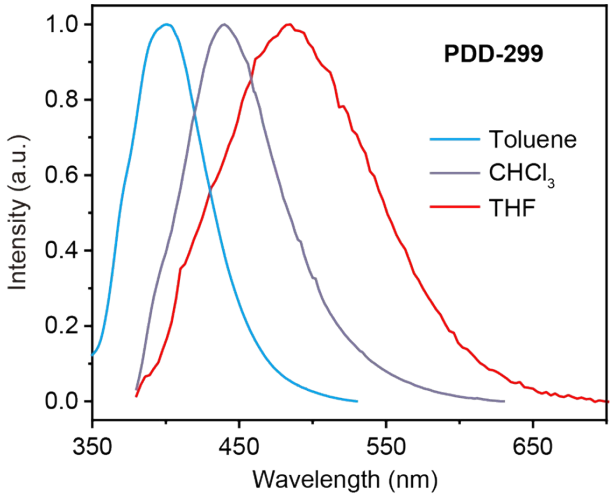

Figure S15. SSPL spectra of **PDD-299** in toluene, trichloromethane and THF (~0.5 mg/mL) at room temperature.

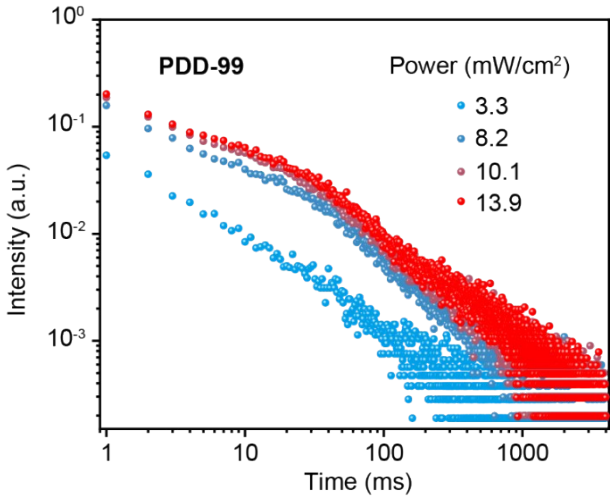

Figure S16. OLPL decay profiles of **PDD-99** powder upon excitation at different power under ambient conditions.

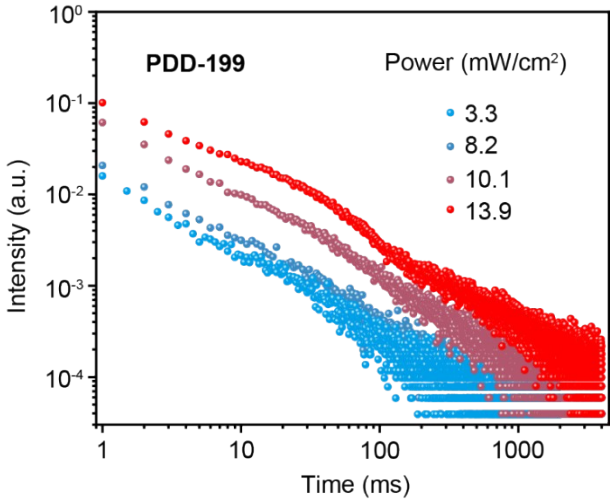

Figure S17. OLPL decay profiles of **PDD-199** powder upon excitation at different power under ambient conditions.

Table S3. The lifetime and PLQY of **PDD-99**, **PDD-199** and **PDD-299** powders under 410 nm excitation.

Materials	Lifetime (ms)	PLQY (%)
PDD-99	485	26.78
PDD-199	492	27.93
PDD-299	515	28.82

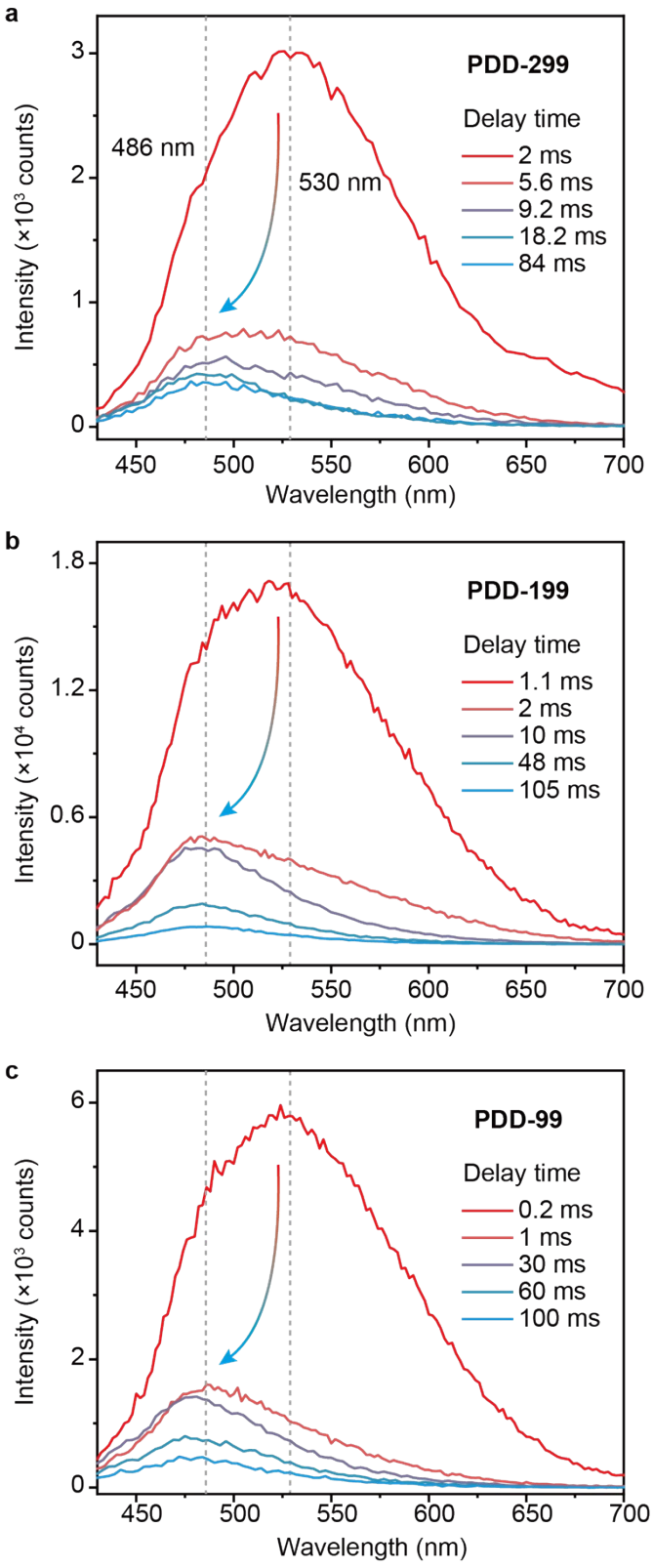

Figure S18. Time resolved phosphorescence spectra of **PDD-299**, **PDD-199** and **PDD-99** (λ_{ex}=410 nm) under ambient conditions.

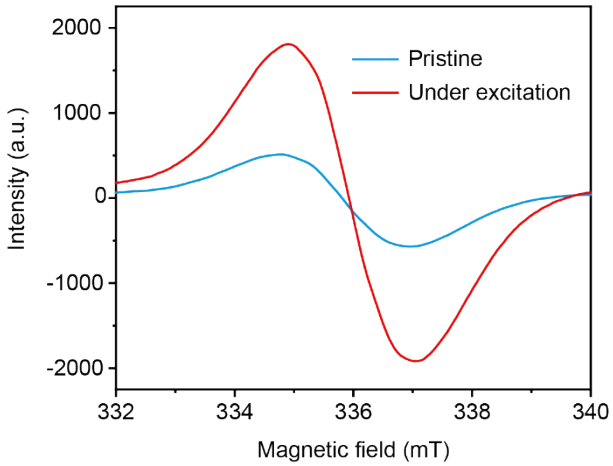

Figure S19. Experimental EPR spectra of **PDD-299** before and after UV excitation.

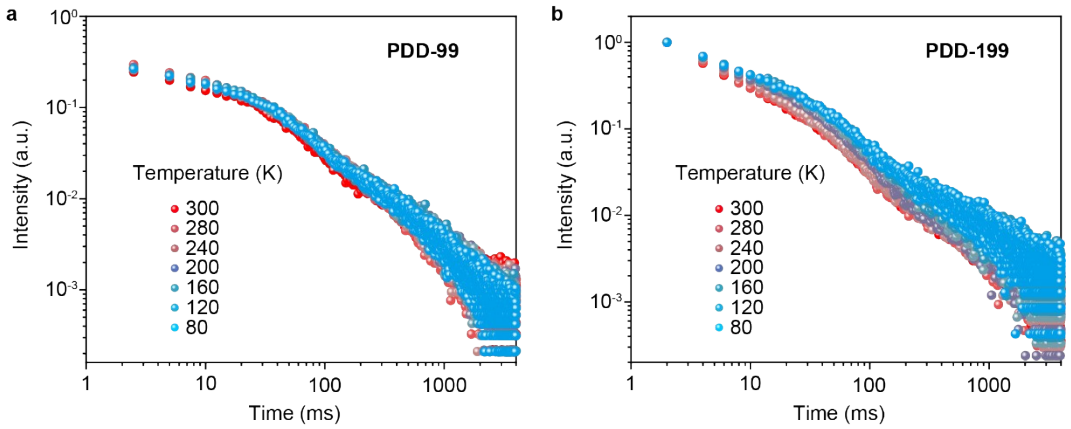

Figure S20. Temperature-dependent OLPL decay profiles (λ_{em}=486 nm) of (a) **PDD-99** and (b) **PDD-199** ranging from 80 to 300 K.

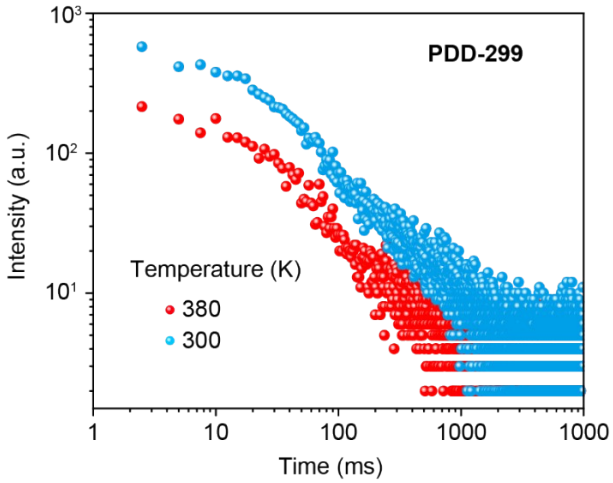

Figure S21. OLPL decay profiles (λ_{em}=486 nm) of **PDD-299** at 300 and 380 K.

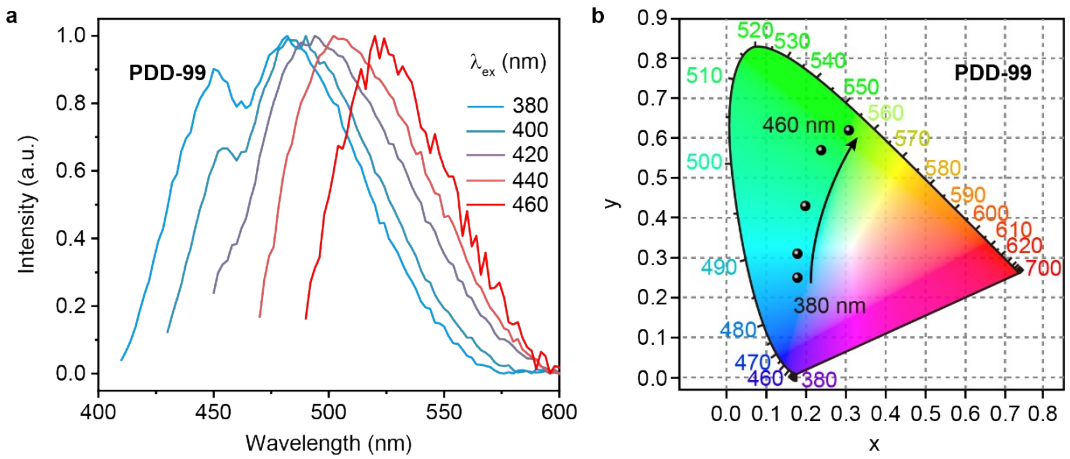

Figure S22. (a) OLPL spectra and (b) CIE coordinates of **PDD-99** powder upon excitation at different wavelength under ambient conditions.

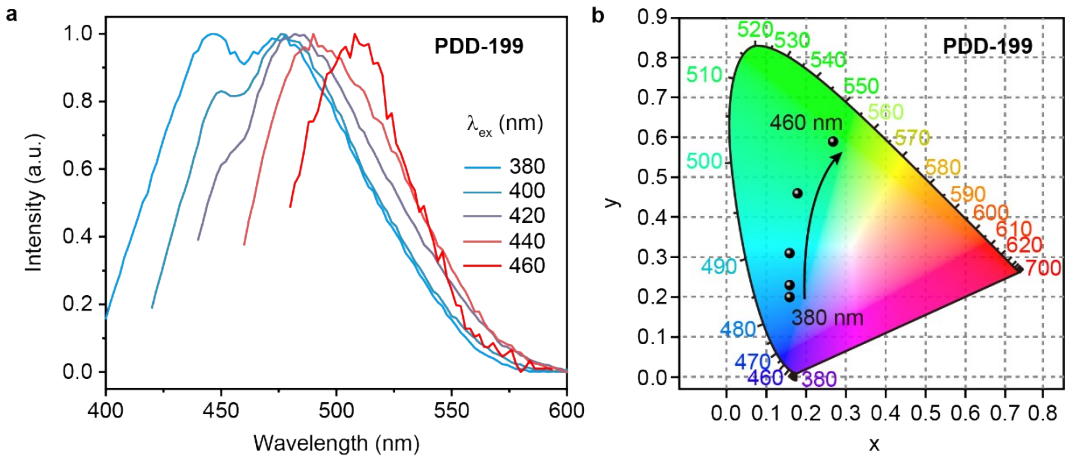

Figure S23. (a) OLPL spectra and (b) CIE coordinates of **PDD-199** powder upon excitation at different wavelength under ambient conditions.

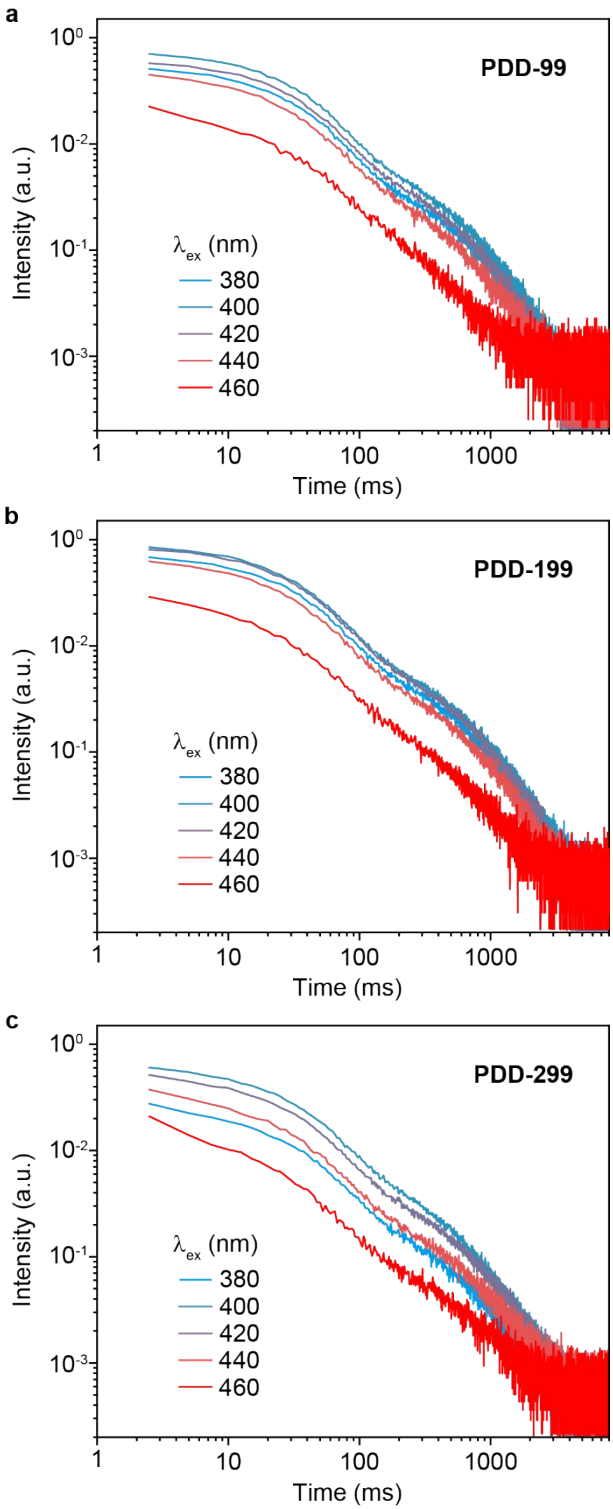

Figure S24. OLPL decay profiles of (a) **PDD-99**, (b) **PDD-199** and (c) **PDD-299** excited by different wavelengths.

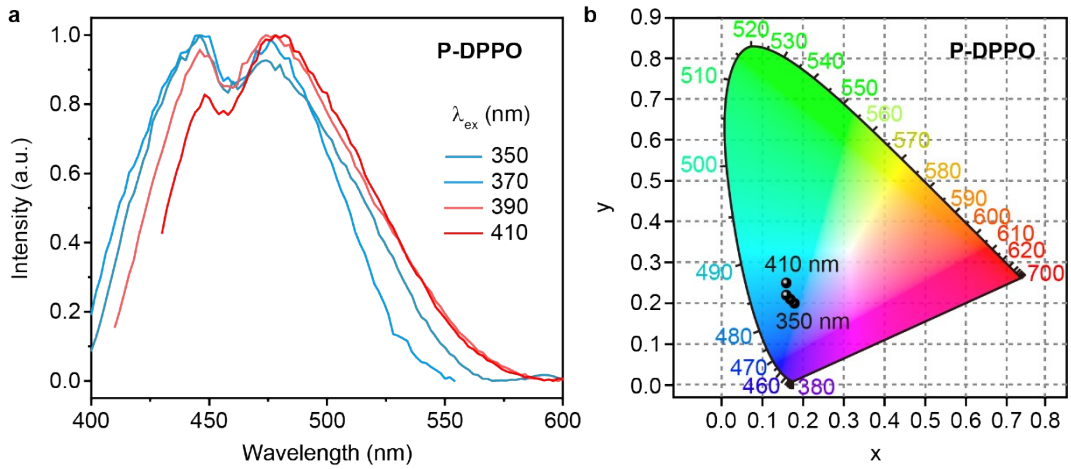

Figure S25. (a) OLPL spectra and (b) CIE coordinates of **P-DPPO** powder upon excitation at different wavelength under ambient conditions.

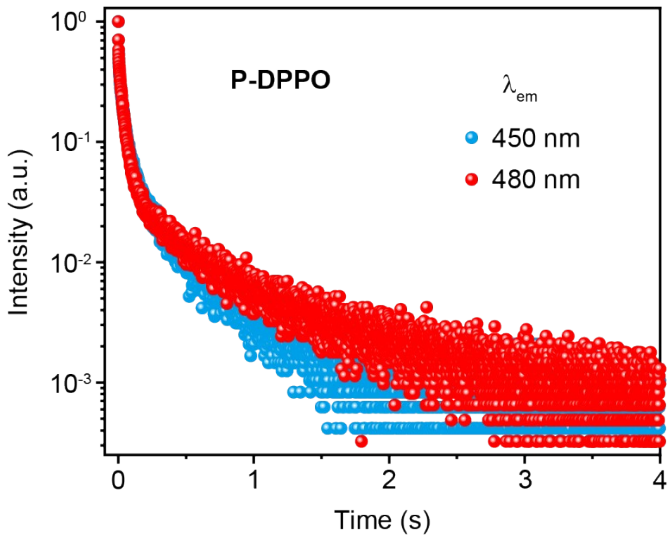

Figure S26. Lifetime decay profiles of emission bands at 450 and 480 nm of **P-DPPO** powder under ambient condition.

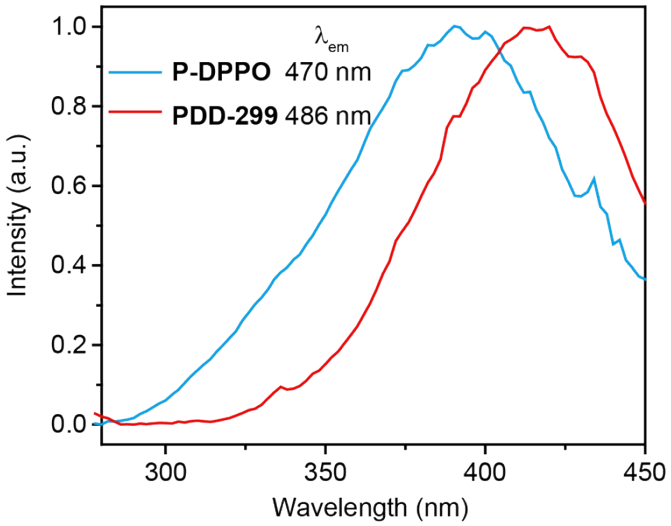

Figure S27. Excitation spectra of **P-DPPO** and **PDD-299** powders by monitoring SSPL peaks of 470 and 486 nm, respectively.

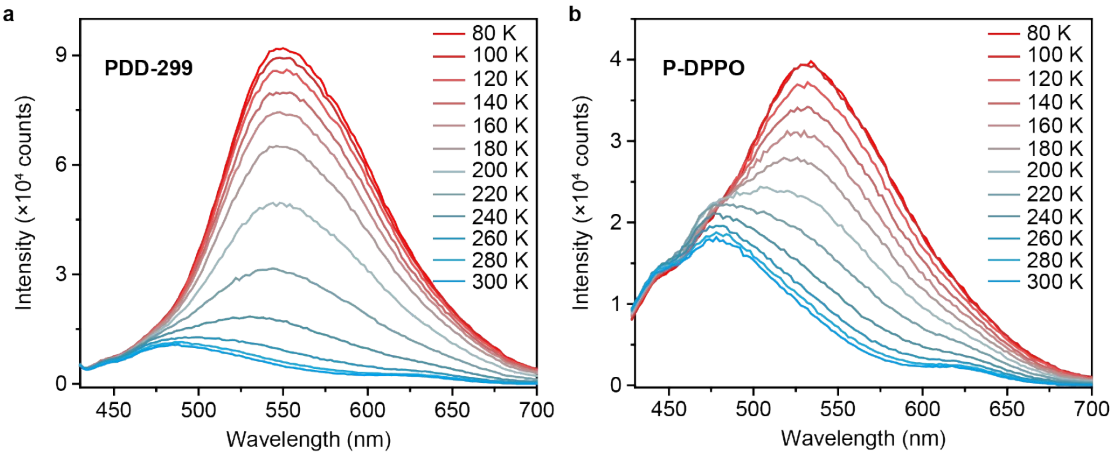

Figure S28. Temperature-dependent phosphorescence spectra (delayed time: 10 ms) of (a) **PDD-299** and (b) **P-DPPO** powders from 300 to 80 K.

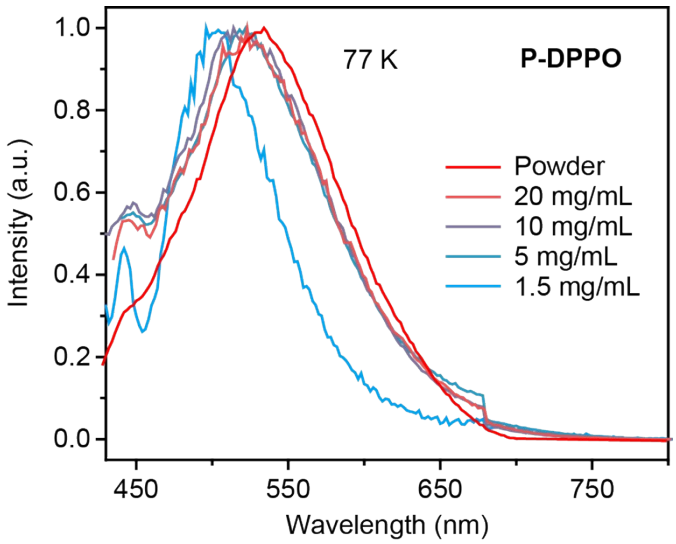

Figure S29. Phosphorescence spectra of **P-DPPO** powder and **P-DPPO** in dichloromethane solutions with varied concentrations of 20, 10, 5 and 1.5 mg/mL excited by 400 nm at 77 K.

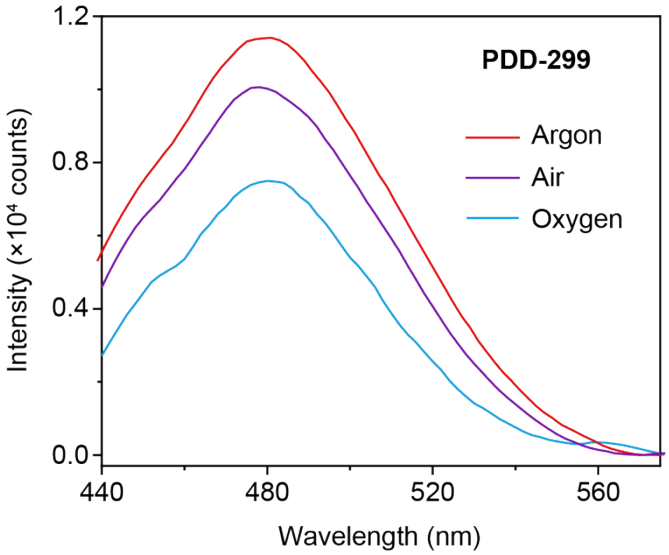

Figure S30. OLPL spectra (delayed time: 10 ms) of **PDD-299** in different atmosphere excited by 410 nm.

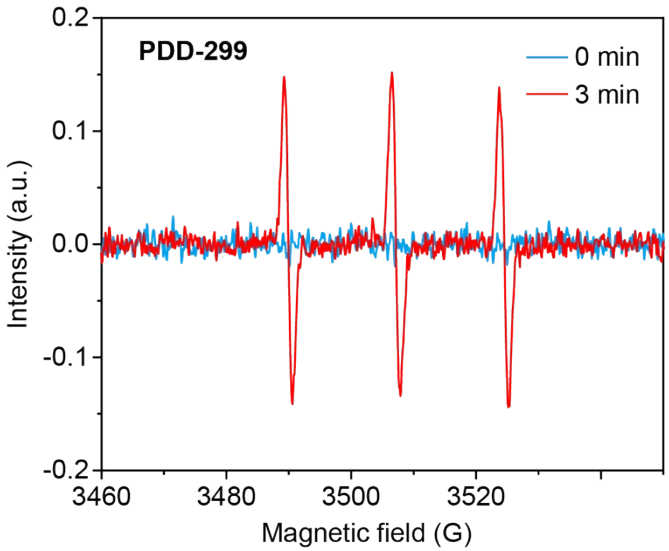

Figure S31. EPR spectra of **PDD-299** in the presence of TEMPO before and after UV light irradiation.

7. Application

In vitro antibacterial performance of PDD-299. The antibacterial efficacy of **PDD-299** on planktonic *Escherichia coli* (*E. coli*, ATCC25922) was assessed. Cultured in Luria-Bertani (LB) medium to the logarithmic growth phase, *E. coli* was then adjusted to a concentration of 2×10^8 CFU/mL. For the assay, 100 μL of this suspension was combined with 100 μL of PDD-299, resulting in a final concentration of 200 μg/mL. The mixture was exposed to visible light from a xenon lamp, emitting at 400 nm with an optical power density of 0.2 W/cm^2, for 10 minutes followed by a 4 h incubation. Afterward, the samples were serially diluted, cultured on LB agar, and incubated at 37°C for 18 h before CFU enumeration. Furthermore, SEM analysis was conducted to observe any morphological changes in *E. coli* (~10^7 CFU/mL) treated with **PDD-299** at a concentration of 200 μg/mL, using the same lighting conditions. Post-treatment, the samples were fixed in 2.5% glutaraldehyde, sequentially dehydrated in ethanol, lyophilized, and then gold-sputtered for SEM examination.

Table S4. A brief summary of the recently reported high-performance in vitro antibacterial materials.

Sample Name	Bacteria Type	Light	Irradiation Time	Antibacterial Efficiency	Ref.
PDD-299	*E. coli*	400 nm	10 min	78.24%	This work
PLNPs@PAA/ CaP-DOX	MRSA	650±10 nm	10 min	40% (pH 7.4), 99% (pH 5.5)	[1]
SeDCz NCs	*S. aureus*	400-800 nm	15 min	~99%	[2]
CNDs	*B. subtilis* and *E. coli*	365 nm	1 h	94%, 93%	[3]
BP/BQD	*S. aureus* and *E. coli*	UV light	15 min	~100%	[4]
BF@AgNPs	*S. aureus* and *E. coli*	visible-light	1 h	~100%	[5]

Reference

1 X. Fu, X. Zhao, L. Chen, P. Ma, T. Liu and X. Yan, *Biomater. Sci.*, 2023, **11**, 5186-5194.

2 L. Xu, K. Zhou, H. Ma, A. Lv, D. Pei, G. Li, Y. Zhang, Z. An, A. Li and G. He, *ACS Appl. Mater. Interfaces*, 2020, **12**, 18385-18394.

3 Y. Miao, X. Zhang, J. Li, W. Yang, X. Huang and J. Lv, *RSC Adv.*, 2022, **12**, 20481-20491.

4 C. Chao, L. Kang, W. Dai, C. Zhao, J. Shi, B. Tong, Z. Cai and Y. Dong, *J. Mat. Chem. B*, 2023, **11**, 3106-3112.

5 Y. Cai, W. Cheng, C. Ji, Z. Su and M. Yin, *Dyes Pigment.*, 2021, **195**, 109698.